Paleontological Research, vol. 24, no. 3, pp. 216–225, July 1, 2020

doi:10.2517/2019PR013

Shell area–to-volume ratio in ammonoids

HORACIO PARENT[1], MATIAS BEJAS[2] AND ANDRES GRECO[2]

[1]*Laboratorio de Paleontología, IFG-FCEIA, Universidad Nacional de Rosario, Pellegrini 250, 2000 Rosario, Argentina (e-mail: parent@fceia.unr.edu.ar)*
[2]*Departamento de Física and Instituto de Física de Rosario, CONICET, Universidad Nacional de Rosario, Pellegrini 250, 2000 Rosario, Argentina.*

Received December 19, 2018; Revised manuscript accepted June 16, 2019

Abstract. The external area-to-volume ratio of the ammonite shell has been held to be related to morphology but never evaluated quantitatively. A dimensionless ratio, the Vogel number, was computed for large samples of Devonian to Cretaceous ammonites with a new method based on the ADA-model. The estimated ratios range from 2.4 to 3.4. The highest values are exhibited by uncoiled serpenticone ammonites, lowering in the sequence serpenticone-oxycone-spherocone. It is shown that the area-to-volume relationships are controlled by the involution (degree of overlapping) and the relative width of whorl section. The typical evolutionary trends serpenticone–spherocone and/or serpenticone–oxycone, broadly documented through the history of the Ammonoidea, could have been driven, at least in part, by the lowering of the area-to-volume ratio.

Key words: Ammonoidea, Devonian–Cretaceous, dimensionless area-to-volume ratio, life history, morphology

Introduction

Ammonoids are cephalopods with an external shell consisting of a more or less tightly coiled cone, in most of which the whorls overlap. The degree of overlapping (involution) and the shape of the whorl section determine a variety of planispiral shell morphotypes (Figure 1A) and submorphotypes. These morphotypes range through a continuous spectrum of uncoiled slender shells (uncoiled serpenticones), barely coiled shells (serpenticones), up to tightly coiled with successive whorls overlapped, inflated (spherocones) or compressed and high-whorled (oxycones). The classification of morphotypes, derived from the classic shell dimensions (Figure 1B), can be expanded naming as many submorphotypes as needed (e.g. Westermann, 1996; Kutygin, 1998; Parent *et al.*, 2010; Klug *et al.*, 2015a).

It has been held that the more involute ammonites (spherocones and oxycones) need a lesser amount of shell wall for enclosing a given volume than the more evolute ones (serpenticones), i.e., that the former have the lower shell area-to-volume ratio (e.g. Raup, 1967; Guex, 2001, 2003; Klug and Korn, 2004; Hammer and Bucher, 2006). A low ratio should have been advantageous for the animal, especially by optimal use of shell material (e.g. Heath, 1985), improved streamlining (review in Jacobs and Chamberlain, 1996), and/or higher shell strength. However, the variation of the ratio by increasing involution and inflation of the shell has not been assessed quantitatively.

While the volume of any complete and well prepared ammonite can be directly and easily measured in the laboratory, it is not possible to measure the area of the external surface accordingly, if not by means of some complex technique (e.g. grinding tomography or computed tomography, see Lemanis *et al*., 2016; Hoffmann *et al*., 2018). There are equations available for numerical approximations of the volume and area from sets of geometrical dimensions and parameters (see Moseley, 1938; Raup and Chamberlain, 1967; Raup and Graus, 1972; Graus, 1974; Hutchinson, 2000). Nevertheless, these equations involve a large number of dimensions not clearly related with the classic ones and impossible to obtain if not from specimens little less than perfect. Dommergues *et al.* (2002), in their study of the evolution of size patterns in Early Jurassic ammonites, described a simple way for a rough estimation of shell volume, but the corresponding area cannot be estimated accordingly. The volume and surface area of individual septa of some ammonites have been estimated by different methods (e.g. Lemanis *et al.*, 2016; Hoffmann *et al.*, 2018), but not for the whole shell to our knowledge.

Thus, it should be useful to compute the area-to-volume ratio, especially from the classic dimensions of the ammonite shell. These estimations would allow us to study quantitatively the patterns of variation of the

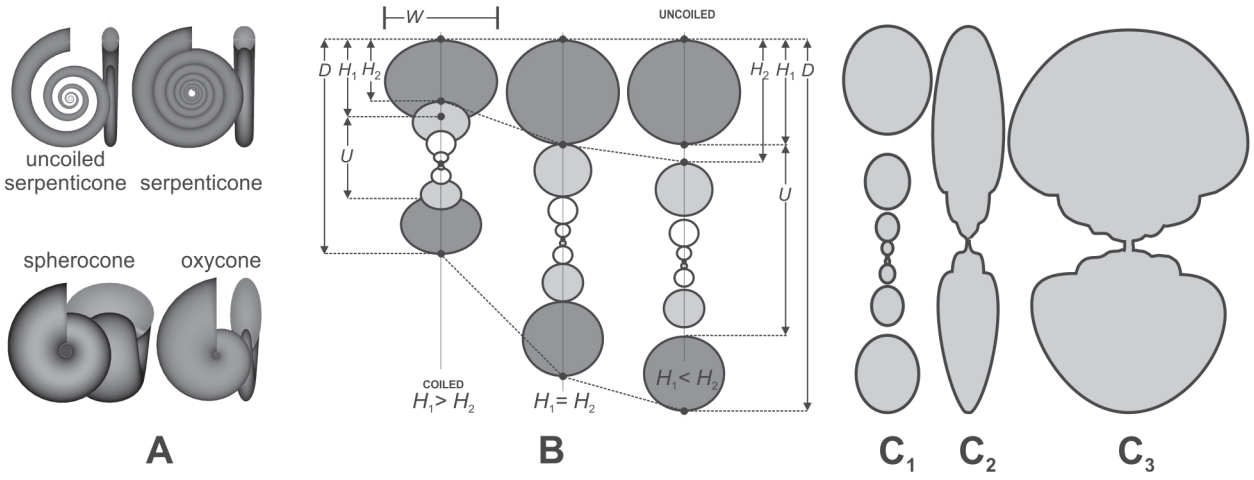

Figure 1. Nomenclature and dimensions adopted in this paper. **A,** morphotype nomenclature. **B,** Classic dimensions of the ammonite shell. The three cross-sections show the relationships between the dimensions through the increase of whorl overlap (involution). Left, coiled shell in which $H_1 > H_2$; center, shell at the threshold $H_1 = H_2$; right, uncoiled shell in which $H_1 < H_2$ (after Parent *et al.*, 2010). **C,** diagrammatic cross section of an uncoiled ammonite (C_1), an oxycone (C_2), and a spherocone (C_3), showing the surface whose area is considered herein as the external area *A* (bold black lines), the area that effectively is in physical contact with the sea water, and gray the encased volume *V*. Note that (1) the dorsal walls are not included in the external surface area *A*, and (2) the external surface area considered in calculations comprises the whole ammonite, from the protoconch.

ratio through the morphologic diversity of the planispiral ammonites. Then, these patterns could be analyzed for potential implications in the life history and evolution of ammonoids.

In this paper we present a new method for computation of a dimensionless external shell area-to-volume ratio which is applied for computing a ratio through a continuum of ammonite morphotypes. Every set of measurements corresponding to each specimen measured is used to obtain, from the ADA-model (Parent *et al*., 2010, 2012), a 3-D model to represent this ammonite; the dimensionless area-to-volume ratio is then computed.

The use of the terms shape and size is explained in Parent *et al.* (2010); the shape of an object encompasses all of its geometric properties except its size (scale), position and orientation (see details in Small, 1996; Klingenberg, 2010). We use the term uncoiled for any curved ammonite, from those openly curved to those with one or more coiled whorls which are not in contact.

Material

The material considered for this study consists of (1) 1222 sets of measurements (*D*, *U*, *W*, H_1, H_2) from 201 species of planispiral Triassic, Jurassic and Cretaceous representative ammonoids used in Parent *et al.* (2010), fitting eq. 1 (below) with a mean relative error between actual and predicted values of 7%; (2) 333 specimens belonging to 116 species of clymeniids and other Devonian, Carboniferous and Permian ammonoids (figured by Petter, 1959, 1960; Gordon, 1964; Nassichuk, 1975; Chlupac and Turek, 1983; Korn, 1997; Leonova, 2011; Bockwinkel *et al.*, 2013), fitting eq. 1 with relative errors of 1–20%. These latter samples of Palaeozoic ammonoids are not an exhaustive representation of the vast universe of these forms, but provide an acceptable representation of most of the known submorphotypes. The group of Palaeozoic ammonoids that grow maintaining the relative umbilical width unchanged through most of their ontogeny is not included in this study.

Dimensionless external shell area-to-volume ratio

Biometric techniques are powerful tools for the study of the great quantity of information the ammonite shell contains, the success of which rests on the adoption of a set of adequate dimensions. By adequate we mean: easy to measure and directly interpretable in quantitative terms and literal descriptions, even from incomplete specimens. In this sense the so-called shell diameter (*D* in Figure 1B) is the most convenient and informative (in field and laboratory) linear dimension for quantification of the ammonite size. The other classic dimensions on which most quantitative studies are based (e.g. Nicolesco, 1927; Bassé, 1952; Enay, 1966; Dagis, 1968; Yacobucci, 2004; Zatón, 2008; Raffi and Olivero, 2016) are (Figure 1B): width (*W*), heigth (H_1) and apertural–height (H_2) of the whorl section, and the umbilical diameter (*U*).

The method for calculation of the external shell area-

to-volume ratio is derived from the ADA-model developed for planispiral ammonites. The kernel of this model is the relationship between the classic dimensions in dimensionless–mode, given by the following equation (see Appendix 1, and Parent *et al.*, 2010, 2012 for derivation):

$$\text{(eq. 1)} \quad \frac{U}{D} = 1 - 2\frac{H_1}{D} + \left(\frac{H_1}{D}\right)^2 \frac{H_2}{H_1}$$

We have based the present study on the ADA-model because (1) the classic ammonite shell dimensions are related by a single equation, (2) coiled and uncoiled (planispiral) forms share a single morphospace modelled by the same single equation, (3) the fields of geometrically possible and not-possible ammonites is not speculative but exact, and (4) it can be applied to simple direct measurements from imperfect and/or incomplete specimens, and with no special preparation. It is important here that the ADA-model allows us to evaluate the contribution of the shell dimensions to shape and size, as well as their relationships (morphology). The ammonite shell shape is mainly controlled by the degree of whorl overlap (ratio between apertural whorl height and total whorl height: H_2/H_1, see Figure 1B) following an approximate central morphogenetic rule $H_2/D = 0.3$ (Figure 2A: bold gray curve). The variety of morphologies is generated by the interplay between the degree of whorl overlap, the relative total whorl height (H_1/D), and the relative whorl width (W/D). The distribution of, and the relationships among the different morphotypes (serpenticone, spherocone, oxycone) and submorphotypes can be well represented in the reduced morphospaces **RM1** = {H_2/H_1, H_1/D} and **RM2** = {H_2/H_1, W/D} (Figure 2), thus showing the covariation of the degree of whorl overlap, whorl section shape and relative umbilical diameter. Of great importance is that the ADA-model has allowed identifying the size (represented by D) as the definite constraint that explains the nonexistence (at least not known) of many geometrically possible ammonites (Parent *et al.*, 2010).

The shell area-to-volume ratio is usually defined by means of the ratio between both dimensions (e.g. Thompson, 1917; Gould, 1966; Sprent, 1972), but it is well known that this ratio A/V is lower in larger forms. In terms of the framework of the ADA-model, the Vogel number (see Vogel, 1981), $V_N = A^{1/2}/V^{1/3}$, is a simple and convenient dimensionless number for quantification, defined by the shell shape independently of size. The area A considered is that of the external surface of the whole shell, that which is effectively in physical contact with the sea water; the volume V corresponds to the space delimited by the external surface of the shell (Figure 1C).

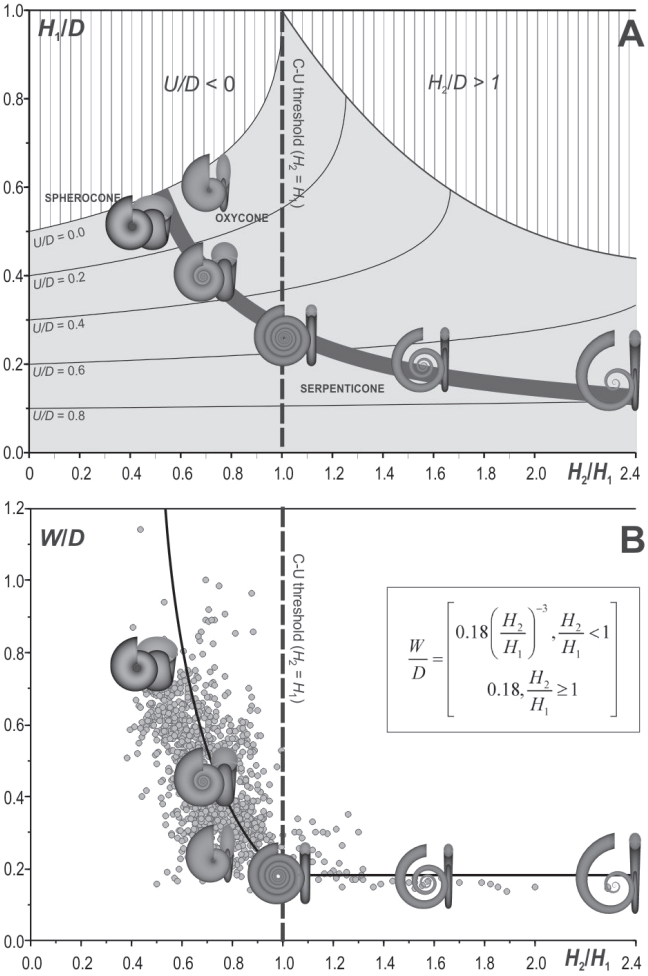

Figure 2. Reduced morphospaces of the ADA-model. **A,** distribution of morphotypes in the reduced morphospace **RM1** = {H_2/H_1, H_1/D} with indication of the U/D-gradient determined by eq. 1. The bold gray curve indicates the main pattern or trend which corresponds to ammonites with a relative apertural height $H_2/D = 0.3$. The H_2/H_1-axis is truncated for representation, it has no limit tending to infinity as shells are straighter. The C–U threshold ($H_1 = H_2$) is the limit between the fields of coiled and uncoiled geometries. Gray field for geometrically possible morphologies, although known ammonites do not depart far from the main trend because of the constraint of size (diameter). Vertical gray-shaded indicates the fields where ammonites are geometrically impossible. **B,** distribution of morphotypes in the reduced morphospace **RM2** = {H_2/H_1, W/D}. The curve is defined by the equation in the inset.

As described in Parent *et al.* (2010), the 3-D models of ammonite shells are created by placing ellipses in the center of the logarithmic spiral $r(\theta) = c \cdot e^{\lambda\theta}$ (Figure 3A). The axes of the ellipse are $a_1(\theta) = m \cdot e^{\lambda\theta}$ and $a_2(\theta) = t \cdot a_1(\theta)$. The parameters c, m, λ, and t are related to H_2/H_1, H_1/D, and W/D as indicated in Appendix 1.

Using the equations in Appendix 1 for sets of measure-

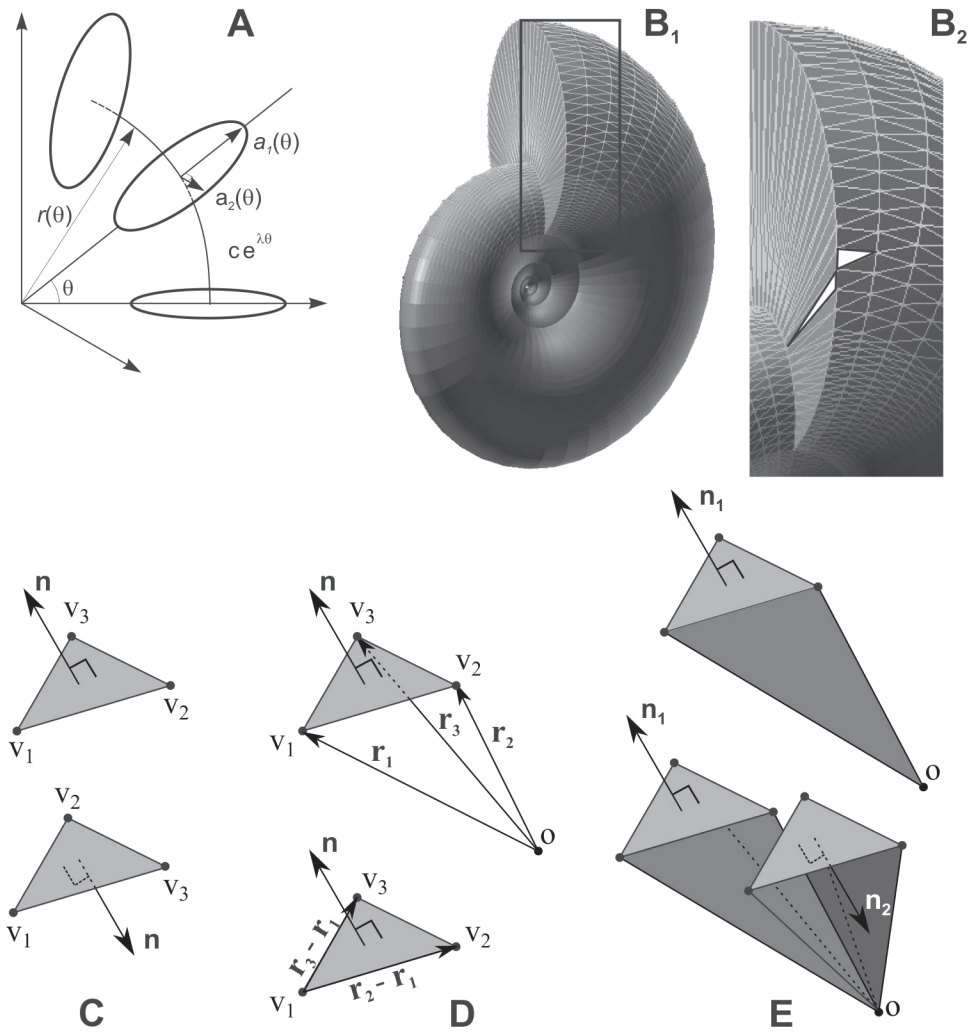

Figure 3. Vectorial geometric elements for modelling ammonite shells (A) and computation of the external shell area-to-volume ratio (B–E). **A,** parameters and variables defined in the ADA-model for modelling a theoretical ammonite as explained in the text and Appendix 1. **B,** theoretical ammonite showing the partitions for computation of the external area *A* and volume *V* (B_1); the rectangle in B_1 corresponds to the enlarged view in B_2 where the two white triangles are examples. Note that the external area considered comprises the whole ammonite, from the protoconch if laterally exposed (see Figure 1C). **C,** elementary triangles in B. **D,** elementary triangles and vectors defined for calculation of the area. **E,** elementary prisms and vectors defined for calculation of the volume. Explanation in the text.

ments of H_2/H_1, H_1/D, W/D, we produce three-dimensional ammonite-shell models. Since we are interested in the dimensionless quantity V_N the size of the 3-D model is irrelevant. It was adopted $c = 1$ for the 3-D representations.

Computation of *A* and *V* is based on the 3-D model as built by triangles (Figure 3B). Each triangle (T) is formed by three vertices (v) and is noted as $T_1 = (v_1, v_2, v_3)$. A vector named **n** (normal to the surface of the triangle) indicates the front face of the triangle. The direction of **n** is obtained from the right-hand rule following the order of the vertices that define the triangle (Figure 3C).

Computation of the external area: Each vertex v_i has a coordinate $\mathbf{r_i}$ with respect to the origin o of the coordinate system. The vectors that go from one vertex to another can be computed as the difference between the coordinates of each vertex. For instance, the vector ($\mathbf{r_3} - \mathbf{r_1}$) in the figure goes from vertex v_1 to v_3, and the vector ($\mathbf{r_2} - \mathbf{r_1}$) goes from vertex v_1 to v_2 (Figure 3D). The area of the triangle can be computed taking the module of the cross product between these two vectors.

$$\textit{area of the triangle} = \left(\frac{1}{2}\right)\left|\left(\mathbf{r}_2 - \mathbf{r}_1\right)\times\left(\mathbf{r}_3 - \mathbf{r}_1\right)\right|$$

The sum of the area of all these triangles is the external

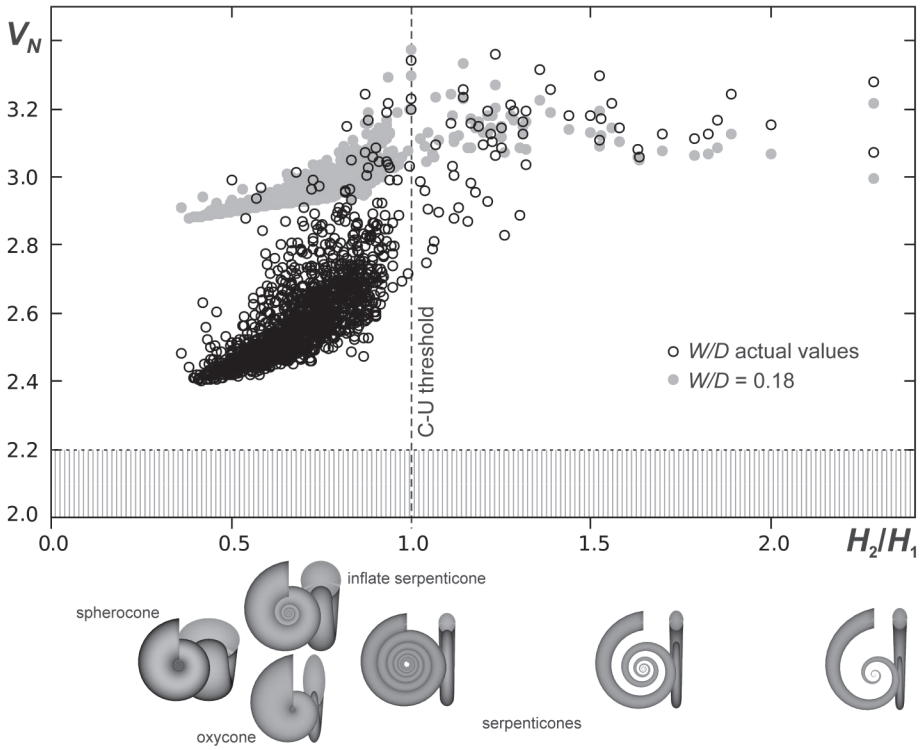

Figure 4. External shell area-to-volume ratio V_N for the studied sample of ammonites (open circles) computed with the actual values. The strong effect of the progressive inflation of the shell lowering V_N is illustrated by the high values obtained after computing the ratio with a fixed value $W/D = 0.18$ (gray points). The C–U threshold $H_1 = H_2$ is the limit between coiled and uncoiled geometries (coiled and uncoiled fields). The simulated ammonites below the *x*–axis are distributed according to its involution value of H_2/H_1. The limit 2.2 is the value of the sphere below which no other shape is conceived.

area of the ammonite shell.

Computation of the volume: The volume is computed by adding the volumes of the prisms formed by each triangle and the origin of the coordinate system. The volume of each prism formed by the triangles whose faces point away from o will be added, and those which point towards o will be subtracted (Figure 3E). The volume of the prism, taking in account the sign, formed by the triangle (v_1, v_2, v_3) and the point o is computed as:

$$\textit{volume of the prism} = \left(\frac{1}{6}\right)\mathbf{r}_1 \cdot \left[\left(\mathbf{r}_2 - \mathbf{r}_1\right) \times \left(\mathbf{r}_3 - \mathbf{r}_1\right)\right]$$

There are a number of shell features which are not included in our model: (1) The sculpture (ribs, keels and/or spines) if not extremely prominent would produce non-significant changes in the area-to-volume ratio, (2) the volume considered here is just that of the shell and does not include the part of the soft body (in some including the aptychi) which can be projected out of the shell in moments of maximum activity (see Parent *et al.*, 2014; Parent and Westermann, 2016), and (3) in lappeted microconchs the functional area and volume of the shell could be slightly different from that calculated here since the lappets seem to actually represent incomplete segments of the shell (see Klug *et al.*, 2015c).

Results

The V_N values obtained from our model are plotted in Figure 4. These results show that the increase of whorl overlap (lowering of H_2/H_1) produces the reduction of the external shell area-to-volume ratio. Additionally, the increase of relative whorl section width (W/D) leads to further lowering of the ratio. In this form the involute and inflated shells have the lowest area-to-volume ratios. Serpenticonic (including those that are uncoiled) shells have the highest values of V_N whereas those that are oxyconic have lower values and spherocones the lowest. These lowest values of V_N are not far from that of a sphere (2.2) which for a given volume is the shape that has the smallest surface area.

The influence of W/D in lowering the ratio is very significant as illustrated in Figure 4, showing the computa-

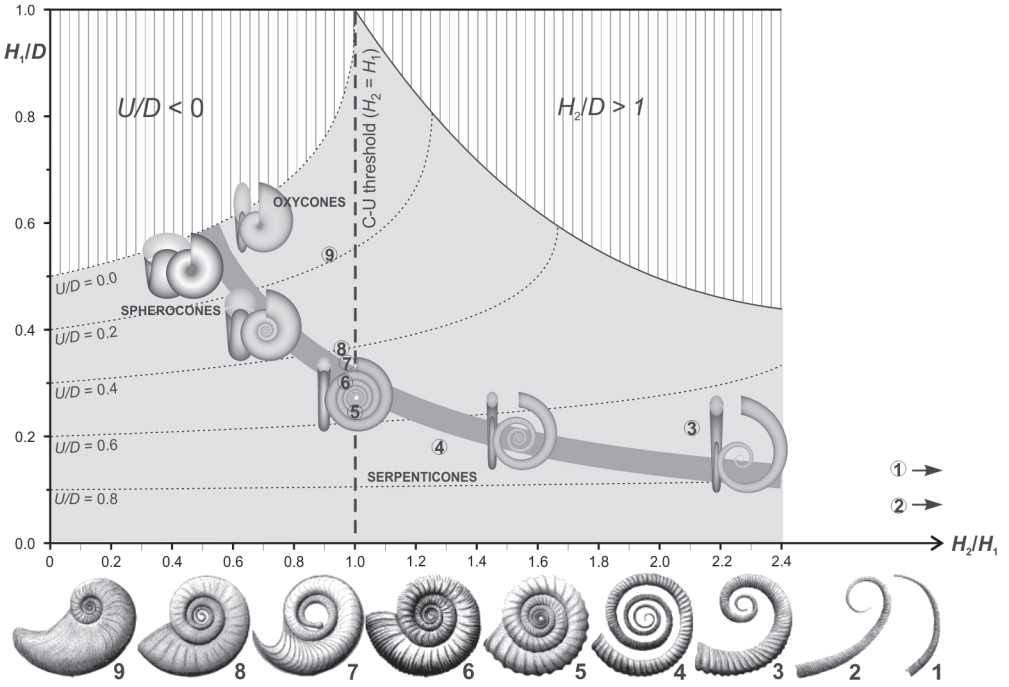

Figure 5. Early evolution of the Ammonoidea represented in the main morphospace $\{H_2/H_1, H_1/D\}$. Note that the shell-shape trend of the lineage follows rather quietly the main trend $H_2/D = 0.3$ (bold gray line) which is associated with the reduction of V_N according to Figure 4. Selected specimens and evolutionary pattern modified from De Baets *et al.* (2013). **1,** *Cyrtobactrites asinuatus*; **2,** *Metabactrites fuchsi*; **3,** *Ivoites schindewolfi*; **4,** *Anetoceras mittmeyeri*; **5,** *Erbenoceras solitarium*; **6,** *Mimosphinctes tripartitus*; **7,** *Gyroceratites heinrichi*; **8,** *Teicherticeras*? sp.; **9,** *Mimagoniatites fecundus*. Cases 1 and 2 are as much uncoiled as to fall out of the represented range of the H_2/H_1-axis. Case 9 is located in an extreme position due to the adult modification of its outermost whorl.

tion of V_N in two ways for the whole sample: (1) with constant $W/D = 0.18$ (which is the almost constant value in uncoiled to barely coiled serpenticones; see Figure 2B) and (2) with the actual values of W/D. This latter way of computation of the ratio V_N, from the actual measurements, produces much lower values, showing the strong influence of the inflation of the shell.

There seems to be a maximum V_N in ammonites of about 3.4, and a minimum of about 2.4. The marked fall of V_N in the vicinity of the threshold $H_2/H_1 = 1$ (Figure 4) is clearly a consequence of the overlapping between the subsequent whorls which are also relatively wider (see Figure 2).

The morphogenetic rule or pattern represented by the curve $H_2/D = 0.3$ in the morphospace of the ADA-model (Figure 2A) is associated with the pattern of variation of the area-to-volume ratio in terms of the whorl overlap (H_2/H_1).

Discussion

Lower area-to-volume ratios in involute ammonites and the apparent implications have been assumed and discussed by several authors (e.g. Guex, 2001, 2003, 2006; Klug and Korn, 2004; Monnet *et al.*, 2015). The estimations presented here provide an accurate quantification of this pattern in the morphospace of the planispiral ammonoids. A variant from the generally assumed pattern is that the oxycones which are generally considered to have a high area-to-volume ratio (Guex, 2003), actually have relatively low values (Figure 4).

Heath (1985) and Hutchinson (2000) have pointed out that there is an optimum overlap which minimises the amount of shell material required to enclose a particular volume in gastropod shells. The problem considered for these latter authors is similar to that studied here through V_N. We have shown that V_N is mainly controlled by the involution or degree of overlap (H_2/H_1), nevertheless, since the relative whorl width (W/D) also has a strong influence, there is an optimum value of overlap for each value of W/D.

The shell area and volume must have been crucial features of the ammonoid life history. This is suggested by the following considerations. The construction of the shell implies an important metabolic compromise (e.g. Bucher *et al.*, 1996) mainly represented by the external shell area, since the dorsal wall and the thin septa represent a much smaller part (see Kulicki *et al*., 2001; Radtke

and Keupp, 2017). Low ratios allow for optimization in the use of shell material, and thus are favourable in terms of metabolic efficiency. On the other hand, the shell area and volume had critical influence in the hydrodynamic properties (see Trueman, 1941; Jacobs and Chamberlain, 1996; Naglik *et al.*, 2015). Thus, the area-to-volume ratio must have represented at every moment in the life of the animal an outcome of the compromise between these two features, a tradeoff that must have had great influence in the evolution of the life history of ammonoids (cf. Tendler *et al*., 2015; Klug *et al*., 2016).

The swimming abilities and capabilities of ammonoids depended on many factors. Jacobs and Chamberlain (1996) have pointed out that most shell shapes may have advantages depending on the size and swimming velocity. There is no room here for discussing this topic at length, but it must be noted that the drag is in great part a function of the external shell area, and lower area-to-volume ratios imply lower areas for a given volume. Among ammonites with the same volume, those with lower V_N have a smaller external area. However, the frictional drag acting on the surface is negligible in the high Reynolds number region in which an adult ammonoid swims. The predominant drag force in such a case is the form drag which does not act on the external shell surface. This indicates that the area-to-volume ratio would be not important for hydrodynamics of large ammonoids. The ratio is important for a juvenile ammonoid with a small diameter swimming slowly. Hatchling juveniles are generally spherical in shape in order to minimize the area-to-volume ratio, while many ammonoids species develop more compressed shell shapes in the later growth stage (Jacobs and Chamberlain, 1996).

The early evolution of the Ammonoidea in the Devonian was dominated by a gradual increase of coiling of the shell (Figure 5), from an almost straight-shelled ancestor (updated review in Klug *et al.*, 2015b and references therein). Later, during the history of the Ammonoidea, phyletic trends of shell shape from evolute serpenticones towards more involute spherocones and oxycones have been recurrent. These trends have been documented in a large number of phylogenetically distant lineages at several different time periods (e.g. Erben, 1966; Donovan, 1985; Dommergues, 1990; Guex, 1992, 2001, 2006; Monnet *et al.*, 2011, 2015). The causes and mechanisms that have produced the trend of increasing shell involution in ammnoids remain to be studied in detail. Nevertheless, assuming that the tradeoff represented by the external shell area-to-volume ratio was significant in the life history of ammonoids, it could mean that those commonly observed phyletic trends reflect persistent trends of lowering this ratio.

Conclusion

From the ADA-model, the ratio between the external area and volume of planispiral ammonite shells was computed in the form of the Vogel number. In Palaeozoic and Mesozoic ammonites, the V_N is the lowest for the more involute and inflated ammonites, the spherocones which are not far from that of a sphere (V_N = 2.2). Oxycones also have low values but, although lower than serpenticones, theirs are higher than in spherocones. Inflated serpenticones have similar V_N to oxycones.

The evolution of the wide morphospace of ammonite shell shapes was determined by the increase of the shell involution, *i.e.*, the reduction of H_2/H_1. The increase of involution and relative whorl width led to the reduction of the external shell area-to-volume ratio in planispiral ammonites.

Decoupling between volume and size in ammonites has been proposed by Guex (2003), concluding that it generates the increasing of the involution. Our results suggest a somewhat different explanation: the increase of involution makes it possible for the morphogenetic program to decouple the area-to-volume ratio from size increase.

The lowering of the ratio through most phyletic trends in the history of the Ammonoidea, shows that this condition must have been clearly favourable for several aspects of the life history of planispiral ammonoids; it is even possible that these trends were driven, among other factors, by the reduction of the external shell area-to-volume ratio.

Acknowledgements

The journal editors, Yasunari Shigeta and Takao Ubukata, as well as two anonymous reviewers have contributed to improving the manuscript of this paper.

References

Bassé, E., 1952: Sous-classe des Ammonoidea. *In*, Piveteau, J. *ed.*, *Traité de Paléontologie*, p. 522–555. Masson et Cie, Paris.

Bockwinkel, J., Becker, R. T. and Ebbighausen, V., 2013: Late Givetian ammonoids from Hassi Nebech (Tafilalt Basin, Anti-Atlas, southern Morocco). *Fossil Record*, vol. 16, p. 5–65.

Bucher, H., Landman, N. H., Klofak, S. M. and Guex, J., 1996: Mode and rate of growth in ammonoids. *In*, Landman, N. H., Tanabe, K. and Davis, R. A. *eds*., *Ammonoid Paleobiology*, p. 407–461. Topics in Geobiology, vol. 13, Plenum, New York.

Chlupac, I. and Turek, V., 1983: Devonian goniatites from the Barrandian area, Czechoslovakia. *Rozpravy Ústředního Ústavu Geologického*, vol. 46, p. 1–159.

Dagis, A. A., 1968: Toarcian ammonites (Dactylioceratidae) from Siberia. *Trudy Instituta Geologii i Geofiziki*, vol. 40, p. 1–108.

De Baets, K., Klug, C., Korn, D., Bartels, C. and Poschmann, M., 2013: Emsian Ammonoidea and the age of the Hunsrück Slate (Rhenish Mountains, western Germany). *Palaeontographica*, *Abteilung A*,

vol. 299, p. 1–113.
Dommergues, J.-L., 1990: Ammonoids. *In*, McNamara, K. *ed*., *Evolutionary Trends*, p. 162–187. Belhaven Press, London.
Dommergues, J.-L., Montuire, S. and Neige, P., 2002: Size patterns through time: the case of the Early Jurassic ammonite radiation. *Paleobiology*, vol. 28, p. 423–434.
Donovan, D. T., 1985: Ammonite shell form and transgression in the British Lower Jurassic. *In*, Bayer, U. and Seilacher, A. *eds*., *Sedimentary and Evolutionary Cycles*. Lecture Notes in Earth Sciences, p. 48–57. Springer-Verlag, Berlin.
Enay, R., 1966: L'Oxfordien dans la moitié sud du Jura français. *Nouvelles Archives du Muséum d'Histoire Naturelle de Lyon*, vol. 8, p. 1–624.
Erben, H. K., 1966: Über den Ursprung der Ammonoidea. *Biological Reviews*, vol. 41, p. 641–658.
Gordon, M., 1964: Carboniferous cephalopods of Arkansas. *U. S. Geological Survey Professional Paper*, 460, p. 1–322.
Gould, S. J., 1966: Allometry and size in ontogeny and phylogeny. *Biological Reviews*, vol. 41, p. 587–640.
Graus, R. R., 1974: Latitudinal trends in the shell characteristics of marine gastropods. *Lethaia*, vol. 7, p. 303–314.
Guex, J., 1992: Origin of the evolutionary jumps in ammonoids. *Bulletin de la Société Vaudoise des Sciences Naturelles*, vol. 82, p. 117–144.
Guex, J., 2001: Environmental stress and atavism in ammonoid evolution. *Eclogae Geologicae Helvetiae*, vol. 94, p. 321–328.
Guex, J., 2003: A generalization of the Cope's rule. *Bulletin de la Société Géologique de France*, vol. 174, p. 449–452.
Guex, J., 2006: Reinitialization of evolutionary clocks during sublethal environmental stress in some invertebrates. *Earth and Planetary Science Letters*, vol. 242, p. 240–253.
Hammer, Ø. and Bucher, H., 2006: Generalized ammonoid hydrostatics modelling, with application to *Intornites* and intraspecific variation in *Amaltheus*. *Paleontological Research*, vol. 10, p. 91–96.
Heath, D. J., 1985: Whorl overlap and economical construction of the gastropod shell. *Biological Journal of the Linnean Society*, vol. 24, p. 165–174.
Hoffmann, R., Lemanis, R. E., Falkenberg, J., Schneider, S., Wesendonk, H. and Zachow, S., 2018: Integrating 2D and 3D shell morphology to disentangle the palaeobiology of ammonoids: a virtual approach. *Palaeontology*, vol. 61, p. 89–104.
Hutchinson, J. M. C., 2000: Three into two doesn't go: two-dimensional models of bird eggs, snail shells and plant roots. *Biological Journal of the Linnean Society*, vol. 70, p. 161–187.
Jacobs, D. K. and Chamberlain, J. A. Jr., 1996: Buoyancy and hydrodynamics in Ammonoids. *In*, Landman, N. H., Tanabe, K. and Davis, R. A. *eds*., *Ammonoid Paleobiology*, p. 169–224. Topics in Geobiology, vol. 13, Plenum, New York.
Klingenberg, C. P., 2010: Evolution and development of shape: integrating quantitative approaches. *Nature Review Genetics*, vol. 11, p. 623–635.
Klug, C., De Baets, K. and Korn, D., 2016: Exploring the limits of morphospace: Ontogeny and ecology of late Viséan ammonoids from the Tafilalt, Morocco. *Acta Palaeontologica Polonica*, vol. 61, p. 1–14.
Klug, C. and Korn, D., 2004: The origin of ammonoid locomotion. *Acta Palaeontologica Polonica*, vol. 49, p. 235–242.
Klug, C., Korn, D., Landman, N. H., Tanabe, K., De Baets, K. and Naglik, C., 2015a: Describing ammonoid conchs. *In*, Klug, C., Korn, D., De Baets, K., Kruta, I. and Mapes, R. H. *eds*., *Ammonoid Paleobiology: From Anatomy to Ecology*. Topics in Geobiology, vol. 43, p. 3–24. Springer, Heidelberg.
Klug, C., Kröger, B., Vinther, J., Fuchs, D. and De Baets, K., 2015b: Ancestry, origin and early evolution of ammonoids. *In*, Klug, C., Korn, D., De Baets, K., Kruta, I. and Mapes, R. H. *eds*., *Ammonoid Paleobiology: From Macroevolution to Paleogeography*. Topics in Geobiology, vol. 44, p. 3–24. Springer, Heidelberg.
Klug, C., Zatoń, M., Parent, H., Hostettler, B. and Tajika, A., 2015c: Mature modifications and sexual dimorphism. *In*, Klug, C., Korn, D., De Baets, K., Kruta, I. and Mapes, R. H. *eds*., *Ammonoid Paleobiology: From Anatomy to Ecology*. Topics in Geobiology, vol. 43, p. 253–320. Springer, Heidelberg.
Korn, D., 1997: The Palaeozoic ammonoids of the South Portuguese Zone. *Memórias do Instituto Geológico e Minero*, vol. 33, p. 1–131.
Kulicki, C., Tanabe, K., Landman, N. H. and Mapes, R. H., 2001: Dorsal shell wall in ammonoids. *Acta Palaeontologica Polonica*, vol. 46, p. 23–42.
Kutygin, R. V., 1998: Shell shapes of Permian ammonoids from northeastern Russia. *Paleontological Journal*, vol. 32, p. 20–31.
Lemanis, R., Korn, D., Zachow, S., Rybacki, E. and Hoffmann, R., 2016: The evolution and development of cephalopod chambers and their shape. *PlosOne*, vol. 11, doi:10.1371/journal.pone.0151404.
Leonova, T. B., 2011: Permian ammonoids: biostratigraphic, biogeographical and ecological analysis. *Paleontological Journal*, vol. 45, p. 1206–1312.
Monnet, C., De Baets, K. and Klug, C., 2011: Parallel evolution controlled by adaptation and covariation in ammonoid cephalopods. *BMC Evolutionary Biology*, vol. 11, doi:10.1371/journal.pone.0151404.
Monnet, C., Klug, C. and De Baets, K., 2015: Evolutionary patterns of ammonoids: phenotypic trends, convergence, and parallel evolution. *In*, Klug, C., Korn, D., De Baets, K., Kruta, I. and Mapes, R. H. *eds*., *Ammonoid Paleobiology: From Macroevolution to Paleogeography*. Topics in Geobiology, vol. 44, p. 95–142. Springer, Heidelberg.
Moseley, H., 1838: On the geometrical forms of turbinated and discoid shells. *Philosophical Transactions of the Royal Society of London*, vol. 128, p. 351–370.
Naglik, C., Tajika, A., Chamberlain, J. and Klug, C., 2015: Ammonoid locomotion. *In*, Klug, C., Korn, D., De Baets, K., Kruta, I. and Mapes R. H. *eds*., *Ammonoid Paleobiology: From Anatomy to Ecology*. Topics in Geobiology, vol. 43, p. 649–688. Springer, Heidelberg.
Nassichuk, W. W., 1975: Carboniferous ammonoids and stratigraphy in the Canadian Arctic Archipelago. *Geological Survey of Canada Bulletin*, no. 237, p. 1–240.
Nicolesco, C. P., 1927: Etude monographique du genre *Parkinsonia*. *Mémoires de la Société Géologique de France*, *new series*, vol. 9, p. 1–85.
Parent, H., Bejas, M., Greco, A. and Hammer, Ø., 2012: Relationships between dimensionless models of ammonoid shell morphology. *Acta Palaeontologica Polonica*, vol. 57, p. 445–447.
Parent, H., Greco, A. F. and Bejas, M., 2010: Size-shape relationships in the Mesozoic planispiral ammonites. *Acta Palaeontologica Polonica*, vol. 55, p. 85–98.
Parent, H. and Westermann, G. E. G., 2016: Jurassic ammonite aptychi: Functions and evolutionary implications. *Swiss Journal of Palaeontology*, vol. 135, p. 101–108.
Parent, H., Westerman, G. E. G. and Chamberlain, J. A. Jr., 2014: Ammonite aptychi: Functions and role in propulsion. *Geobios*, vol. 47, p. 45–55.
Petter, G., 1959: Goniatites dévoniennes du Sahara. *Publications du Service de la Carte Géologique de l'Algérie*, *nouvelle série*, *Paléontologie*, mémoire 2, p. 1–313.
Petter, G., 1960: Clyménies du Sahara. *Publications du Service de*

la Carte Géologique de l'Algérie, *nouvelle série*, *Paléontologie*, mémoire 6, p. 1–58.
Radtke, G. and Keupp, H., 2017: The dorsal shell wall structure of Mesozoic ammonoids. *Acta Palaeontologica Polonica*, vol. 62, p. 59–96.
Raffi, M. E. and Olivero, E. B., 2016: The ammonite genus *Gaudryceras* from the Santonian–Campanian of Antarctica: systematics and biostratigraphy. *Ameghiniana*, vol. 53, p. 375–396.
Raup, D. M., 1967: Geometric analysis of shell coiling: coiling in Ammonoids. *Journal of Paleontology*, vol. 41, p. 43–65.
Raup, D. M. and Chamberlain, J. A. Jr., 1967: Equations for volume and center of gravity in ammonoid shells. *Journal of Paleontology*, vol. 41, p. 566–574.
Raup, D. M. and Graus, R. R., 1972: General equations for volume and surface area of a logarithmically coiled shell. *Mathematical Geology*, vol. 4, p. 307–316.
Small, C. G., 1996: *The Statistical Theory of Shape*, 227 p. Springer-Verlag, New York.
Sprent, P., 1972: The mathematics of size and shape. *Biometrics*, vol. 28, p. 23–37.
Tendler, A., Mayo, A. and Alon, U., 2015: Evolutionary tradeoffs, Pareto optimality and the morphology of ammonite shells. *BMC Systems Biology*, vol. 9, p. 9–12.
Thompson, D'A. W., 1917: *On Growth and Form*, 793 p. Cambridge University Press, Cambridge.
Trueman, A. E., 1941: The ammonite body-chamber, with special reference to the buoyancy and mode of life of the living ammonite. *Quarterly Journal of the Geological Society*, vol. 96, p. 339–383.
Vogel, S., 1981: *Life in Moving Fluids: the Physical Biology of Flow*, 467 p. Princeton University Press, Princeton.
Westermann, G. E. G., 1996: Ammonoid life and habitat. *In*, Landman, N. H., Tanabe, K. and Davis, R. A. *eds*., *Ammonoid Paleobiology*, p. 607–707. Topics in Geobiology, vol. 13. Plenum, New York.
Yacobucci, M. M., 2004: Buckman's Paradox variability and constraints on ammonoid ornament and shell shape. *Lethaia*, vol. 37, p. 57–69.
Zatón, M., 2008: Taxonomy and palaeobiology of the Bathonian (Middle Jurassic) tulitid ammonite *Morrisiceras*. *Geobios*, vol. 41, p. 699–717.

Author contributions

H. Parent: initiated the study, and contributed in all aspects of the study and preparation of the manuscript.

M. Bejas: developed the method for calculation, and contributed in all aspect of the study and preparation of the manuscript.

A. Greco: contributed in all aspects of the study and preparation of the manuscript.

Appendix 1. Derivation of the equations used for computing the dimensionless external shell area-to-volume ratio known as the Vogel number V_N.

(1) The morphological variables (D, H_1, H_2, W) as functions of the modelling variables (c, m, λ, t).

For coiled and uncoiled shells (Figure A1A–B):

(eq. A1) $D(\theta) = (c + m)(1 + e^{-\lambda\pi})e^{\lambda\theta}$

(eq. A2) $H_2(\theta) = (c + m)(1-e^{-2\lambda\pi})e^{\lambda\theta}$

(eq. A3) $W(\theta) = 2tme^{\lambda\theta}$

For uncoiled shells:

(eq. A4) $H_1(\theta) = 2me^{\lambda\theta}$

For coiled shells the value depends on the intersection of two ellipses.

We then compute the intersection between two ellipses, one centred at (x_{0A}, 0), major axis a_{1A}, minor axis a_{2A} = t a_{1A}, and the other at (x_{0B}, 0), minor axis a_{2B} = t a_{1B}, respectively (see Figure A1C).

The equation of the ellipses is $(x - x_{0A})^2 + \frac{y^2}{t^2} = a_{1A}^2$, $(x - x_{0B})^2 + \frac{y^2}{t^2} = a_{1B}^2$. Then, replacing $x_{0B} = r(\theta-2\pi)$, $a_{1B} = a_1(\theta-2\pi)$, $x_{0A} = r(\theta)$, $a_{1A} = a_1(\theta)$:

(eq. A5) $[x - r(\theta - 2\pi)]^2 + \frac{y^2}{t^2} = a_1^2(\theta - 2\pi)$

(eq. A6) $[x - r(\theta)]^2 + \frac{y^2}{t^2} = a_1^2(\theta)$.

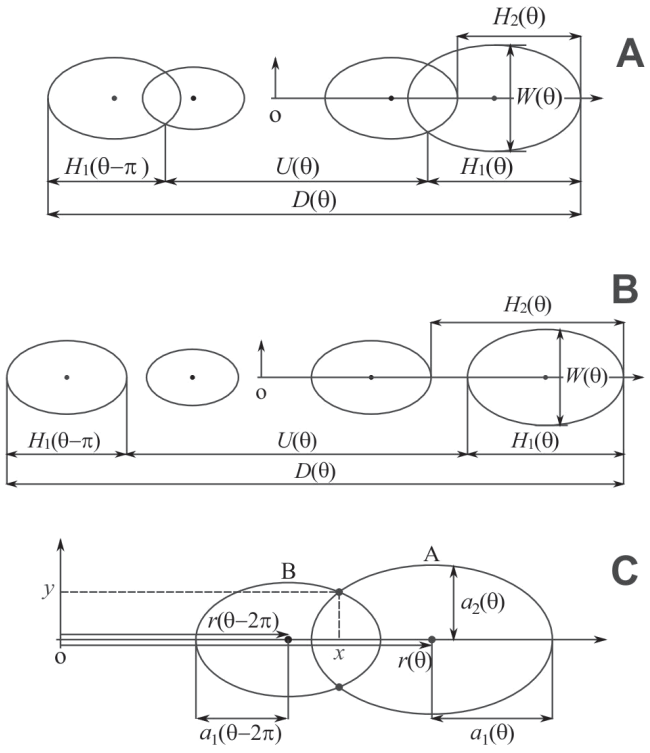

Figure A1. Morphological and modelling variables. **A**, morphological variables for coiled shells; **B**, morphological variables for uncoiled shells; **C**, modelling variables for coiled shells.

The points (x, y) that satisfy eq. A5 correspond to the left-hand ellipse, and those which satisfy eq. A6 to the right-hand ellipse in Figure A1C. The intersection point is at the (x, y) that satisfies both equations. Solving for x the system eqs. A5–A6 we obtain:

$$\text{(eq. A7)} \quad 2x = \frac{[a_1^2(\theta - 2\pi) - a_1^2(\theta) - r^2(\theta - 2\pi) + r^2(\theta)]}{[r(\theta) - r(\theta - 2\pi)]}$$

Note that the x-coordinate of the intersection does not depend on the relation between the axes of the ellipse, i.e., on t.

Replacing in eq. A7, $a_1(\theta) = me^{\lambda\theta}$, $a_1(\theta - 2\pi) = me^{\lambda\theta}e^{-2\lambda\pi}$, $r(\theta) = ce^{\lambda\theta}$, $r(\theta - 2\pi) = ce^{\lambda\theta}e^{-2\lambda\pi}$, we obtain

$$\text{(eq. A8)} \quad 2x(\theta) = [(c^2 - m^2)/c](1 + e^{-2\lambda\pi})e^{\lambda\theta}$$

Note that in eq. A8 we explicit the θ dependence of x. Thus, $H_1(\theta)$ for coiled shells can be computed as

$$\text{(eq. A9)} \quad H_1(\theta) = \{c + m - [(c^2 - m^2)/2c](1 + e^{-2\lambda\pi})\}e^{\lambda\theta}$$

(2) ADA-model variables (H_1/D, H_2/H_1, W/D) as a function of the modelling variables (c, m, λ, t).

In order to simplify the notation in this and the following sections we use: $h_2 = H_2/D$, $h_1 = H_1/D$, $w = W/D$, $h_{21} = H_2/H_1$. Note that $(H_2/H_1) = (H_2/D)/(H_1/D)$, or more compactly $h_{21} = h_2/h_1$. In the main text, h_2 is written as $(H_2/H_1)(H_1/D)$ in order to explicitly use the ADA-model dimensionless variables H_2/H_1 and H_1/D which are considered independent.

For coiled and uncoiled shells, from eq. A1 and eq. A2 we have:

$$\text{(eq. A10)} \quad h_2 = 1 - e^{-\lambda\pi}$$

and from eq. A1 and eq. A3:

$$\text{(eq. A11)} \quad w = 2t/[(c/m + 1)(1 + e^{-\lambda\pi})]$$

For uncoiled shells, from eq. A1 and eq. A4

$$\text{(eq. A12)} \quad h_1 = 2/[(c/m + 1)(1 + e^{-\lambda\pi})]$$

For coiled shells, from eq. A1 and eq. A9

$$\text{(eq. A13)} \quad h_1 = [1 - (\tfrac{1}{2})(1 - m/c)(1 + e^{-2\lambda\pi})]/(1 + e^{-\lambda\pi})$$

Note that the dimensionless variables (eqs. A10–A13) do not depend on θ, and the parameters c and m appear as c/m.

(3) Modelling variables (c, m, λ, t) as functions of the ADA-model variables (H_1/D, H_2/H_1, W/D).

From eq. A10 we obtain

$$\text{(eq. A14)} \quad \lambda = -\pi^{-1} \ln(1 - h_2).$$

From the latter we can write $1 + e^{-\lambda\pi} = 1 + (1 - h_2) = 2 - h_2$, and $1 + e^{-2\lambda\pi} = 1 + (1 - h_2)^2 = 2 - 2h_2 + h_2^2$, thus from eq. A14 we obtain, for uncoiled shells

$$\text{(eq. A15)} \quad c/m = 2/[h_1(2 - h_2)] - 1.$$

From eq. A13 we obtain, for coiled shells

$$\text{(eq. A16)} \quad m/c = 1 - [2 - 2h_1(2 - h_2)]/(2 - 2h_2 + h_2^2).$$

Finally from eq. A11 we obtain

$$\text{(eq. A17)} \quad t = (w/2)(c/m + 1)(2 - h_2).$$

Note that the value c/m in eq. A17 is obtained from eq. A15 for uncoiled shells and from eq. A16 for coiled shells.